

MECHANOCHEMICALLY INDUCED SYNTHESIS OF La_2O_3

Saša Zeljković^{1*}, Mladena Malinović¹, Sunčica Sukur¹,
Dragana Gajić¹, Gordana Ostojić², Milica Balaban¹

¹ University of Banja Luka, Faculty of Natural Sciences and Mathematics, Chemistry Study Program,
Mladena Stojanovića 2, 78 000 Banja Luka, Bosnia and Herzegovina

² Alumina Ltd, Karakaj bb, 75400 Zvornik, Bosnia and Herzegovina

* Corresponding author: sasa.zeljkovic@pmf.unibl.org

Abstract: Lanthanum(III)-oxide (La_2O_3) powders were synthesized by a mechanochemically induced solvent-deficient method using lanthanum nitrate, and ammonium bicarbonate as precursors. The precursor mixture was calcined for one hour at either 600 or 800 °C. This study included an investigation of the formation reactions, crystal structure, specific surface area, and optical properties of synthesized La_2O_3 . The proposed mechanism indicates a complex synthesis with several reactions, some of which are mechanochemically induced. The size of the La_2O_3 nanocrystallites, as determined by XRD, is 22.15 ± 3.9 nm (by using the Williamson-Hall plot, it is determined that the strain is 1.4×10^{-3} and crystallite size 30.81 nm) while the specific surface is set to $7.04 \text{ m}^2\text{g}^{-1}$. The direct bandgap value obtained from reflectance measurement is determined to be 5.37 eV.

Keywords: La_2O_3 , solvent deficient synthesis, nanoparticles.

1. INTRODUCTION

Lanthanum-oxide (La_2O_3) is a white, scentless, and thermally stable (melting point 2315 °C) rare earth metal oxide. La_2O_3 is also low-cost, readily accessible, and insoluble in water. Therefore, it is employed in organic synthesis as an efficient heterogeneous catalyst [1]. La_2O_3 has numerous applications in different areas, including ceramic structures and lightweight structural segments in aerospace and electrochemical applications such as fuel cells [2]. Furthermore, La_2O_3 is used for phosphate eradication [3] in biomedical and water treatment and the high refraction optical fibers manufacturing [4].

The research on La_2O_3 and other metal oxides is also significant due to their commercial and environmental advantages as heterogeneous catalysts, especially in comparison to homo-

geneous catalysts. Some of these advantages include facile separation of catalyst from the mixture, recovery of the catalyst with or without regeneration, uncomplicated purification of the recovered methyl esters, reduction of energy consumption by up to 50 %, and minimization of overall production expenditure [5]. According to Zhou et al. [6], nano La_2O_3 catalytic activity is superior to conventional La_2O_3 catalytic activity due to its high basic strength, small particle dimensions, and consequently – large specific surface area.

Up to now, there are reports of different methods for the La_2O_3 nanoparticles synthesis including sol-gel [4], sonochemical [7], solvothermal [8], and hydrothermal [9]. A lately reported solvent-deficient method [10] was applied in our research. This method is economic and more environmentally friendly than other methods due to

the low consumption of chemicals, rapid synthesis, easiness, and capacity to synthesize compounds without the use of traditional solvents. The solvent-deficient method does not require complicated apparatus or setups. After the first report by Smith et al. [10], this method was optimized and applied for the preparation of binary oxides such as Al_2O_3 [11], and CeO_2 [12], and even more complex ones, such as $\text{Ba}_{0.5}\text{Sr}_{0.5}\text{Co}_{0.8}\text{Fe}_{0.2}\text{O}_3$ [13].

This paper describes the solvent-deficient synthesis of nano La_2O_3 followed by the characterization of the samples.

2. EXPERIMENTAL

The chemicals used for the experiment were ammonium bicarbonate, NH_4HCO_3 (CAS: 1066-33-7, VWR Chemicals BDH), lanthanum(III)-nitrate hexahydrate, $\text{La}(\text{NO}_3)_3 \cdot 6\text{H}_2\text{O}$ (98+%, CAS: 10277-43-7, Acros Organics). The precursors were mixed in a mortar for 20 minutes, followed by rinsing with 100 mL of distilled water. After drying at room temperature and then in a laboratory oven at 100 °C, the resulting powder was used for further analysis and measurements.

The calcination of the precursor powder was performed in a Nabertherm L3/11/B180 muffle furnace for one hour at either 600 or 800 °C with a heating/cooling rate of 10 °C min^{-1} .

The simultaneous TGA/DSC of the precursor powder was performed using the NETZSCH STA 449F3 by measuring weight change (TGA) and differential heat flow (DSC) from 20 to 1000 °C, with a 10 °C min^{-1} heating rate, in the air atmosphere.

FTIR spectra of a series of La_2O_3 samples calcined at different temperatures are acquired using a spectrometer IRAffinity-1 (SHIMADZU). Spectra were collected in the spectral range from 4000 to 500 cm^{-1} , with a resolution of 4 cm^{-1} . The solid samples were mixed with KBr and compressed into pellets.

The BET-specific surface area of the calcined powders was determined from N_2 adsorp-

tion at 77 K on a Micromeritics, Gemini VII (multipoint) instrument.

The reflectance spectrum of La_2O_3 was determined using an Agilent Cary 5000 UV-Vis-NIR spectrophotometer, equipped with a DRA-2500 diffuse reflectance accessory. Measurements were performed in the wavelength range from 200 to 800 nm, with a step of 1 nm and a recording speed of 600 nm min^{-1} . The spectrum of commercial PTFE (polytetrafluoroethylene) was used as the baseline.

Phase identification of the samples was conducted with X-ray diffraction (XRD) on a BRUKER ENDEAVOR D8 diffractometer using DIFRAC.EVA software. The measurements were performed from 10° to 70° 2 θ with 0.02° increments. The crystallite size of the investigated samples was estimated using Scherrer's equation. Additionally, the average crystallite size and microstrain value of the La_2O_3 samples were estimated using the Williamson-Hall plot [14].

3. RESULTS AND DISCUSSION

3.1. Nano La_2O_3 preparation and characterization

Upon grinding at room temperature there is a mechanically induced reaction between lanthanum (III)-nitrate hexahydrate, and ammonium bicarbonate. This reaction results in a semiliquid mixture with partially dissolved La^{3+} ions and ammonium nitrate. As confirmed by the *ab initio* quantum mechanical charge field–molecular dynamics (QMCF-MD) approach, lanthanum ions in an aqueous environment are hydrated with three identified hydration spheres [15]. The water rinsing is responsible for NH_4NO_3 removal, and the complex mechanism of LaOHCO_3 formation in presence of CO_2 and OH^- ion is described elsewhere [16]. Figure 1 shows the TGA/DSC curves of the precursor powder and Table I lists measured phase transitions and corresponding mass losses during TGA/DSC measurement.

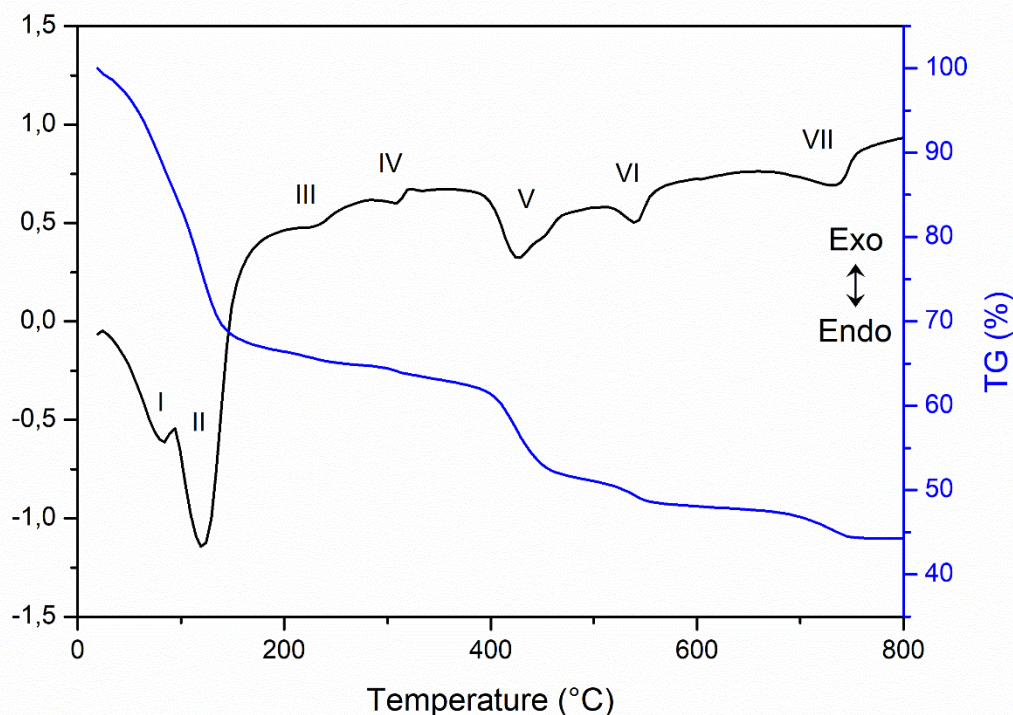


Figure 1. DSC and TGA of the lanthanum(III)-nitrate hexahydrate-ammonium bicarbonate precursor mixture heated to 1000 °C with a 10 °C min⁻¹ heating rate. The seven endothermic peaks correspond to the seven reaction stages, followed by mass reduction

The thermal decomposition of the rinsed and dried precursor mixture (Figure 1) was characterized by an endothermic mass change that can be followed through seven phases, designated as I, II, III, IV, V, VI, and VII. The first study describing the basics of the solvent-deficient method anticipated that rinsed precursors display H₂O and CO₂ byproducts, confirming dehydration/decarbonation reactions occurring. The mass loss observed during TGA/DSC with associated endothermic peaks at 84.2 and 119.2 °C (Phase I and II) in that regard could be associated with the evaporation of residual water and CO₂ and the formation of lanthanum carbonate hydroxide (LaOHCO₃).

Previous research dealing with the preparation and characterization of lanthanum carbonate hydroxide explained the possible existence of two polymorphs having small but different

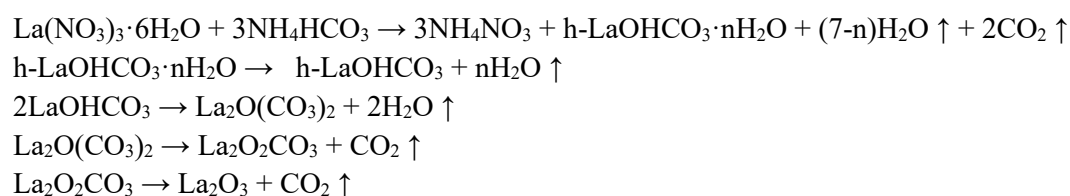
amounts of crystalline water molecule bonded to LaOHCO₃ [17]. Lee et al. [18] studied orthorhombic (o) and hexagonal (h) lanthanum(III)-hydroxy carbonate (LaOHCO₃) further. They found that the polymorph of LaOHCO₃ depended on the reaction temperature, inorganic salt additive, species of Ln³⁺ dopant, and solvent. The observed respective values of x for h- and o-LaOHCO₃·xH₂O were estimated to be 0.73 and 0.25. The authors also noticed that slopes in the followed temperature range indicated that the rate of the LaOHCO₃ to La₂O₂CO₃ conversion is much slower for h- than o-LaCO₃OH. The TG slope in our study is of a pattern similar to the h-LaOHCO₃·xH₂O, which is an indicator of sample composition and behavior within phases III and IV. In that regard, two small endothermic peaks and continuous mass drop could be ascribed to water release from the h-LaOHCO₃·nH₂O molecule.

Table 1. Phase transition and mass losses during TGA/DSC of the lanthanum(III)-nitrate hexahydrate – ammonium bicarbonate precursor mixture heated to 1000 °C with a 10 °C min⁻¹ heating rate

	Temperature (°C)	wt% (weight loss)	Molecular wt. (g mol ⁻¹)	Phase transition	Molecular wt. (g mol ⁻¹)	References
	25 °C 100 °C			$\text{La}(\text{NO}_3)_3 \cdot 6\text{H}_2\text{O} + 3\text{NH}_4\text{HCO}_3 \rightarrow 3\text{NH}_4\text{NO}_3 + \text{h-LaOHCO}_3 \cdot n\text{H}_2\text{O} + (7-n)\text{H}_2\text{O} + 2\text{CO}_2$		This study
I	84.2	33.6%		$\text{CO}_2(\text{aq}) \rightarrow \text{CO}_2 \uparrow$ $\text{H}_2\text{O}(\text{l}) \rightarrow \text{H}_2\text{O} \uparrow$		[10]
II	119.2				[10]	
III	229.2	1.46%		$\text{h-LaOHCO}_3 \cdot n\text{H}_2\text{O} \rightarrow \text{h-LaOHCO}_3 + n\text{H}_2\text{O}$		[17]
IV	309.2	1.95%			[17]	
V	439.2	10.7%	453.76	$2\text{LaOHCO}_3 \rightarrow \text{La}_2\text{O}(\text{CO}_3)_2 + 2\text{H}_2\text{O} \uparrow$	438.30	[22,23]
VI	539.2	3.3%	369.93	$\text{La}_2\text{O}(\text{CO}_3)_2 \rightarrow \text{La}_2\text{O}_2\text{CO}_3 + \text{CO}_2 \uparrow$	369.80	[22,23]
VII	729.2	2.7%	348.60	$\text{La}_2\text{O}_2\text{CO}_3 \rightarrow \text{La}_2\text{O}_3 + \text{CO}_2 \uparrow$	325.80	[22,23]

The question of hydroxycarbonate phase formation and existence was additionally assessed by Colón et al. [19], who were preparing the CeO₂-La₂O₃ catalytic system from nitrate precursors by applying the sol-gel method. They concluded that precipitation with water dissolved ammonia from nitrate solution of rare earth involves the occlusion of anions such as NH₄⁺, NO₃⁻ or CO₃²⁻ and formation of Ln₂(OH)_x(CO₃)_y molecules. The existence of the hydroxy carbonate phase, La₂(OH)_{6-2x}(CO₃)_x, with x ≤ 1, was also suggested by Bernal et al. [20] when lanthanum hydroxide partially transformed into hydroxycarbonate under air atmosphere. Additionally, Kim et al. [21] found out that the thermal decomposition profile of rare-earth hydroxy carbonates is influenced by the decomposition atmosphere and heating rate.

That is why most systematic studies do not necessarily present specific values according to which the onset of thermal decomposition, and therefore trends across the rare earth in general, can be identified. That is also the case in our study, where onset temperatures for observed stages cannot be directly compared to previous results. Further three endothermic weight loss steps have respective maximums of 439.2, 539.2, and 729.2. The observed changes are previously very well described [22,23] and can be related to LaOH(CO₃) losing water (Phase V) followed by La₂O(CO₃)₂ and La₂O₂CO₃ releasing carbon dioxide during respective Phases VI and VII. The joint chemical reaction should include all the above-proposed reactions:



Further examination of La_2O_3 synthesis involved XRD analysis of the material obtained by annealing the precursor in a furnace up to 600 and 800 °C for one hour with a 10 °C min^{-1} heating/cooling rate in the air atmosphere. XRD analysis (Figures 2 and 3) confirmed the presence of La_2O_3 in the sample calcinated at 800 °C. In the sample calcinated at 600 °C, the expected compound was $\text{La}_2\text{O}_2\text{CO}_3$, but because the samples waited for analysis for two months and due to the hygroscopic nature of the material, they were transformed into more stable lanthanum-hydroxide ($\text{La}(\text{OH})_3$). XRD data are provided without data smoothing or background subtraction.

By using Scherrer's equation crystallite size is approximated to be 19.61 ± 7.5 and 22.15 ± 3.9 nm for 600 and 800 °C, respectively. To consider both the effects of strain and size on peak broadening, the Williamson-Hall plot was created based on the Lorentzian function. The strain and crystallite size were calculated from the slope and y-intercept, respectively. For the sample calcinated at 600 °C, the strain was 3.7×10^{-3} and the crystallite size was 55.46 nm. In the case of the sample calcinated at 800 °C, the strain was 1.4×10^{-3} and the crystallite size was 30.81 nm. The crystallite size from the Williamson-Hall plot

is slightly larger than the crystallite size from Scherrer's formula, but still in the range of nanoparticles. The crystal structure of La_2O_3 was confirmed at 800 °C. $\text{La}(\text{OH})_3$ was detected as the second phase in the same sample and its formation is probably a consequence of the hygroscopic nature of La_2O_3 . According to Fleming et al. [24], $\text{La}(\text{OH})_3$ is formed from La_2O_3 promptly after its exposure to air.

The specific surface area (BET) of the material calcined at 600 and 800 °C is found to be 4.51, and 7.04 $\text{m}^2 \text{g}^{-1}$, respectively. The specific surface areas of the samples after calcination are corresponding well to their crystallite size determined by using Scherrer's equation. Zhou et al. [6] have found that the higher specific surface is favorable for La_2O_3 catalytic activity. The high specific surface of La_2O_3 is resulting in better contact with the reactants in the transesterification reaction. In their research, the respective BET surface areas of hydrothermally prepared nano La_2O_3 , sonochemically prepared nano La_2O_3 , and commercially available La_2O_3 were 46.0, 28.3, and 3.3 $\text{m}^2 \text{g}^{-1}$. The BET surface area of La_2O_3 produced by the solvent-deficient method is 7.04 $\text{m}^2 \text{g}^{-1}$, indicating a good possibility for its catalytic activity.

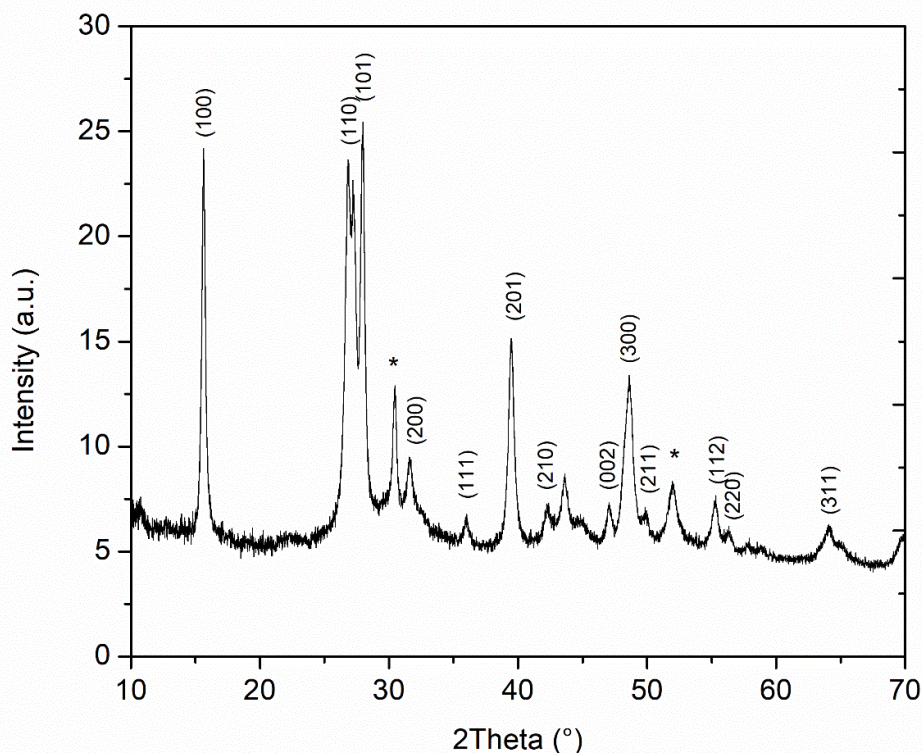


Figure 2. XRD patterns of as-prepared powders were calcined at 600 °C for one hour. The formed $\text{La}(\text{OH})_3$ is present at 600 °C and the Miller indices (JCPDS 36-1481) are denoted above the pattern. $\text{La}(\text{OH})\text{CO}_3$ (JCPDS 26-0815) are denoted by * above the pattern

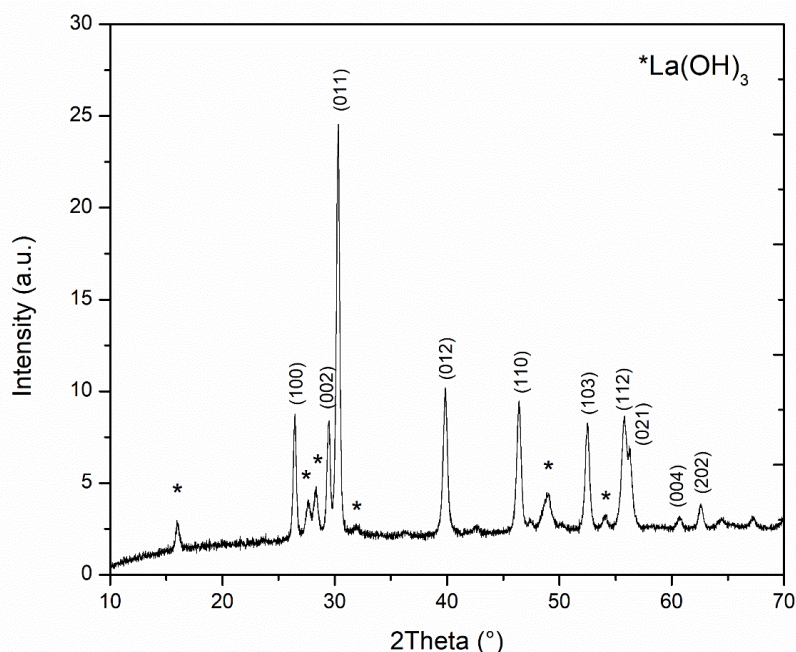


Figure 3. XRD patterns of as-prepared powders were calcined at 800 °C for one hour. The formed La_2O_3 is present at 800 °C and the Miller indices (JCPDS 73-2141) are denoted above the pattern. $\text{La}(\text{OH})_3$ (JCPDS 36-1481) are denoted by * above the pattern

3.2. FTIR analysis

FTIR spectra were recorded to show the functional groups for samples calcinated at various temperatures i.e., 200, 500, 600, and 800 °C (Figure 4).

With increasing calcination temperature, certain evolution of characteristic bands, which can be well related to the results of XRD, was noticeable.

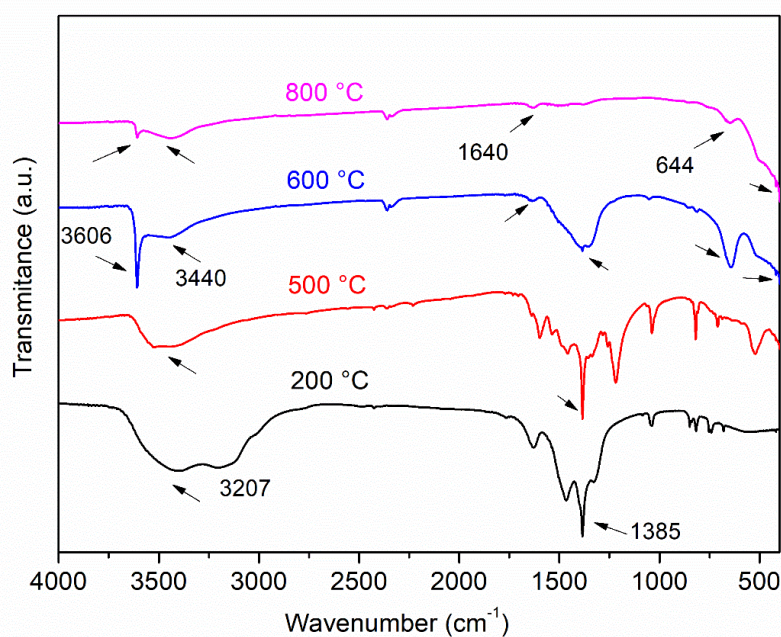


Figure 4. FTIR spectra of the lanthanum(III)-nitrate hexahydrate – ammonium bicarbonate precursor mixture heated for one hour at 200, 500, 600, and 800 °C with a 10 °C min^{-1} heating rate

Due to its basic properties, La_2O_3 is subject to reaction with atmospheric water and CO_2 to form chemisorbed surface types of species. The very characteristic appearance of the area between 3000 and 4000 cm^{-1} in samples calcined at 600 and 800 $^\circ\text{C}$ was observed. A sharp band at 3606 cm^{-1} is assigned to the stretching O–H vibrations of lanthanum hydroxide which is formed by the ageing of La_2O_3 in the air atmosphere [25]. A wide band centered around 3440 cm^{-1} together with a weak band at around 1640 cm^{-1} can be attributed to the O–H vibration and indicate the presence of

adsorbed water on the sample surface. The additional band that appeared at 644 cm^{-1} originated from the La-OH deformation [26]. The broad band centered at 1385 cm^{-1} originated from adsorbed water molecules. The samples calcined at lower temperatures also show a characteristic broad band centered around 3440 cm^{-1} . The additional band at about 3200 cm^{-1} indicates the presence of crystalline carbonate in the sample calcined at 200 $^\circ\text{C}$. By further heating at 400 $^\circ\text{C}$, the sample released crystalline bonded water, and the band at 3200 cm^{-1} disappeared.

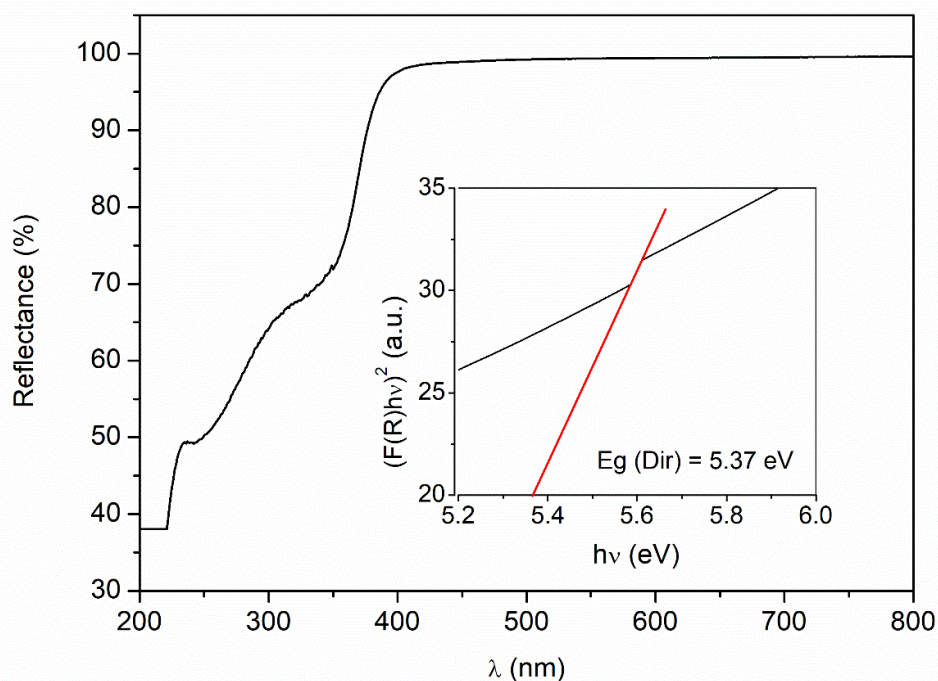


Figure 5. UV-VIS diffuse reflectance spectra of La_2O_3 calcined at 800 $^\circ\text{C}$ for one hour. The inset shows the Kubelka Munk function versus energy plot with an estimated value for a direct bandgap of 5.37 eV

It is well known that the optical properties (including bandgap) of the semiconductor materials correlate with their catalytic activity [27]. The bandgap of the crystalline La_2O_3 calcined at 800 $^\circ\text{C}$ for one hour was examined by the UV–VIS diffuse reflectance spectra (UV-VIS DRS), as shown in Figure 5. The value of the direct band-gap is determined to be about 5.37 eV. This is in good agreement with the values from the literature. Zhao et al. [28] measured the bandgap of the poorly crystallized La_2O_3 film to be approximately 5.3 eV. On the other hand, the direct optical transitions band gap value in La_2O_3 determined by Pandey et al. [29] is estimated to be 5.2 eV. The observed small difference between measured and literature values could be a result of the $\text{La}(\text{OH})_3$

impurities, as well as crystal defects such as vacancies and interstitials, whose presence is previously confirmed by the XRD analysis.

4. CONCLUSIONS

Mechanochemically induced synthesis of nano La_2O_3 is described by a set of chemical reactions based on TG-DSC and FTIR results. Chemical transformation is followed from the mechanochemical reaction at RT and up to 800 $^\circ\text{C}$. The material obtained after one-hour-long heating at either 600 or 800 $^\circ\text{C}$ is inspected by the means of XRD, revealing a multiphase structure. Confirmed $\text{La}(\text{OH})_3$ / $\text{La}(\text{OH})\text{CO}_3$ phases at 600

°C, and $\text{La}_2\text{O}_3 / \text{La}(\text{OH})_3$ phases at 800 °C are most probably the result of two-month-long original material decay. The observed spontaneous reactions to more stable lanthanum compounds are a confirmation of previous findings by several authors. By using Scherrer's equation, the respective crystallite sizes were determined to be 19.61 ± 7.5 and 22.15 ± 3.9 nm for 600 and 800 °C. The strain and crystallite sizes were calculated by using the Williamson-Hall plot. The strain and crystallite sizes were 3.7×10^{-3} and 55.46 nm for the material calcined at 600, and 1.4×10^{-3} and 30.81 nm for the material calcined at 800 °C, respectively. The respective specific surface areas (BET) of the material calcined at 600 and 800 °C are found to be 4.51, and $7.04 \text{ m}^2 \text{ g}^{-1}$. The bandgap of the crystalline La_2O_3 calcined at 800 °C for one hour is by the UV-VIS diffuse reflectance spectra (UV-VIS DRS) determined to be about 5.37 eV. This is in agreement with the literature values.

The described mechanochemically induced synthesis route presents a fast, efficient and reliable way to obtain La_2O_3 nanocrystallites. Future research on La_2O_3 solvent-deficient synthesis should include XRD, SEM, and TEM analysis.

5. ACKNOWLEDGMENTS

This work benefited from networking activities carried out within the EU-funded COST Action CA18112 – "Mechanochemistry for Sustainable Industry" and represents a contribution to it.

6. REFERENCES

- [1] S. U. Tekale, V.P. Pagore, S. S. Kauthale, R. P. Pawar, *La₂O₃/TFE: An efficient system for room temperature synthesis of Hantzsch polyhydroquinolines*, Chin. Chem. Lett., Vol. 25 (2014) 1149–1152.
- [2] L. Lili, T. Jie, L. Yuxiang, Z. Mei, W. Xidong, *Synthesis and thermodynamic analysis of nano-La₂O₃*, Prog. Nat. Sci., Vol 17 (2007) 838–844.
- [3] L. Lai, Q. Xie, L. Chi, W. Gu, D. Wu, *Adsorption of phosphate from water by easily separable Fe₃O₄@SiO₂ core/shell magnetic nanoparticles functionalized with hydrous lanthanum oxide*, J. Colloid Interface Sci., Vol. 465 (2016) 76–82.
- [4] H. Kabir, S. H. Nandyala, M. M. Rahman, M. A. Kabir, A. Stamboulis, *Influence of calcination on the sol-gel synthesis of lanthanum oxide nanoparticles*, Appl. Phys. A., Vol. 124 (2018) 820.
- [5] S. Glišić, I. Lukic, D. Skala, *Biodiesel synthesis at high pressure and temperature: Analysis of energy consumption on industrial scale*, Bioresour. Technol., Vol. 100 (2009) 6347–6354.
- [6] Q. Zhou, H. Zhang, F. Chang, H. Li, H. Pan, W. Xue, D.-Y. Hu, S. Yang, *Nano La₂O₃ as a heterogeneous catalyst for biodiesel synthesis by transesterification of Jatropha curcas L. oil*, J. Ind. Eng. Chem., Vol. 31 (2015) 385–392.
- [7] M. Salavati-Niasari, G. Hosseinzadeh, F. Davar, *Synthesis of lanthanum hydroxide and lanthanum oxide nanoparticles by sonochemical method*, J. Alloys Compd., Vol. 509 (2011) 4098–4103.
- [8] Z. Sun, G. Liu, Z. Fu, T. Sheng, Y. Wei, Z. Wu, *Nanostructured La₂O₃: Yb³⁺/Er³⁺: Temperature sensing, optical heating and bio-imaging application*, Mater. Res. Bull., Vol. 92 (2017) 39–45.
- [9] L. Yu, Y. Han, R. Lin, K. Ge, C. Zhang, J. Zhang, G. Jia, *Controllable synthesis and luminescence properties of one-dimensional La₂O₃ and La₂O₃:Ln³⁺ (Ln = Er, Eu, Tb) nanorods with different aspect ratios*, J. Lumin., Vol. 229 (2021) 117663.
- [10] S. J. Smith, B. Huang, S. Liu, Q. Liu, R. E. Olsen, J. Boerio-Goates, B. F. Woodfield, *Synthesis of metal oxide nanoparticles via a robust "solvent-deficient" method*, Nanoscale, Vol. 7 (2015) 144–156.
- [11] T. Ivas, M. Balaban, V. Dosen, J. Miyawaki, K. Ito, D. Vrankovic, G. Ostojic, S. Zeljkovic, *Optimization of the calcination temperature for the solvent-deficient synthesis of nanocrystalline gamma-alumina*, Chem. Pap., Vol. 73 (2019) 901–907.
- [12] S. Zeljković, D. Jelić, H. Maruyama, J. C. Nino, *Solvent-deficient synthesis of cerium oxide: Characterization and kinetics*, Ceram. Int., Vol. 45 (2019) 10063–10071.
- [13] S. Zeljkovic, J. Miyawaki, D. Vrankovic, E. Tervoort, R. Hauert, T. Kotegawa, T. Ivas, *Solvent-deficient synthesis of nanocrystalline Ba_{0.5}Sr_{0.5}Co_{0.8}Fe_{0.2}O_{3-δ} powder*, Process. Appl. Ceram., Vol. 12 (2018) 342–349.
- [14] M. Ganjali, S. Pourhashem, M. Mozafari, *The effect of heat-treatment on the structural characteristics of nanocrystalline*

chlorapatite particles synthesized via an in situ wet-chemical route, *Ceram. Int.*, Vol. 41 (2015) 13100–13104.

[15] O. M. D. Lutz, T. S. Hofer, B. R. Randolph, B. M. Rode, *Hydration of trivalent lanthanum revisited – An ab initio QMCF-MD approach*, *Chem. Phys. Lett.*, Vol. 536 (2012) 50–54.

[16] G. Tamil Selvi, A. Nirmala Grace, S. K. Jeong, *Synthesis of rare earth hydroxycarbonate (LaOHCO_3) nanocrystals with tuneable morphology and luminescence properties*, *Adv. Powder Technol.*, Vol. 31 (2020) 2366–2378.

[17] J. Sun, T. Kyotani, A. Tomita, *Preparation and characterization of lanthanum carbonate hydroxide*, *J. Solid State Chem.*, Vol. 65 (1986) 94–99.

[18] M. H. Lee, W. S. Jung, *Hydrothermal Synthesis of LaCO_3OH and Ln^{3+} -doped LaCO_3OH Powders under Ambient Pressure and Their Transformation to $\text{La}_2\text{O}_2\text{CO}_3$ and La_2O_3* , *Bull. Korean Chem. Soc.*, Vol. 34 (2013) 3609–3614.

[19] G. Colón, J. A. Navío, R. Monaci, I. Ferino, *CeO_2 – La_2O_3 catalytic system. Part I. Preparation and characterisation of catalysts*, *Phys. Chem. Chem. Phys.*, Vol. 2 (2000) 4453–4459.

[20] S. Bernal, J. A. Diaz, R. Garcia, J. M. Rodriguez-Izquierdo, *Study of some aspects of the reactivity of La_2O_3 with CO_2 and H_2O* , *J. Mater. Sci.*, Vol. 20 (1985) 537–541.

[21] P. Kim, A. Anderko, A. Navrotsky, R. Riman, *Trends in Structure and Thermodynamic Properties of Normal Rare Earth Carbonates and Rare Earth Hydroxycarbonates*, *Minerals*, Vol. 8 (2018) 106.

[22] J. Liu, G. Wang, L. Lu, Y. Guo, L. Yang, *Facile shape-controlled synthesis of*

lanthanum oxide with different hierarchical micro/nanostructures for antibacterial activity based on phosphate removal, *RSC Adv.*, Vol. 7 (2017) 40965–40972.

[23] M. Hämmer, H. A. Höppe, *Crystalline orthorhombic $\text{Ln}[\text{CO}_3][\text{OH}]$ ($\text{Ln}=\text{La}, \text{Pr}, \text{Nd}, \text{Sm}, \text{Eu}, \text{Gd}$) compounds hydrothermally synthesised with CO_2 from air as carbonate source*, *Z. Für Naturforschung B.*, Vol. 74 (2019) 59–70.

[24] P. Fleming, R. A. Farrell, J. D. Holmes, M. A. Morris, *The Rapid Formation of $\text{La}(\text{OH})_3$ from La_2O_3 Powders on Exposure to Water Vapor*, *J. Am. Ceram. Soc.*, Vol. 93 (2010) 1187–1194.

[25] Q. Mu, Y. Wang, *Synthesis, characterization, shape-preserved transformation, and optical properties of $\text{La}(\text{OH})_3$, $\text{La}_2\text{O}_2\text{CO}_3$, and La_2O_3 nanorods*, *J. Alloys Compd.*, Vol. 509 (2011) 396–401.

[26] N. A. Razali, M. Conte, J. McGregor, *The role of impurities in the La_2O_3 catalysed carboxylation of crude glycerol*, *Catal. Lett.*, Vol. 149 (2019) 1403–1414.

[27] A. B. Getsoian, Z. Zhai, A.T. Bell, *Band-Gap Energy as a Descriptor of Catalytic Activity for Propene Oxidation over Mixed Metal Oxide Catalysts*, *J. Am. Chem. Soc.*, Vol. 136 (2014) 13684–13697.

[28] Y. Zhao, K. Kita, K. Kyuno, A. Toriumi, *Band gap enhancement and electrical properties of La_2O_3 films doped with Y_2O_3 as high- k gate insulators*, *Appl. Phys. Lett.*, Vol. 94 (2009) 042901.

[29] A. Pandey, G. Jain, D. Vyas, S. Irusta, S. Sharma, *Nonreducible, Basic La_2O_3 to Reducible, Acidic $\text{La}_{2-x}\text{Sb}_x\text{O}_3$ with Significant Oxygen Storage Capacity, Lower Band Gap, and Effect on the Catalytic Activity*, *J. Phys. Chem. C*, Vol. 121 (2017) 481–489.

МЕХАНОХЕМИЈСКИ ИНДУКОВАНА СИНТЕЗА La_2O_3

Сажетак: Прашкови лантанијум(III)-оксида (La_2O_3) синтетизовани су механохемијски индукованом методом уз недостатак растварача коришћењем лантанијум-нитрата и амонијум-бикарбоната као прекурсора. Смјеша прекурсора калцинирана је један сат на 600 или 800 °C. Ово истраживање је укључило испитивање реакција формирања, кристалне структуре, специфичне површине и оптичких својстава синтетизованог La_2O_3 . Предложени механизам указује на сложену синтезу са неколико реакција, од којих су неке механохемијски индуковане. Величина нанокристалног La_2O_3 , одређена XRD-ом, износи $22,15 \pm 3,9$ nm (коришћењем Вилијамсон-Хол графикана утврђено је да је микронапрезање $1,4 \times 10^{-3}$ и величина кристалита 30,81 nm), док је специфична површина била $7,04 \text{ m}^2\text{g}^{-1}$. Вриједност директног енергетског процјепа добијена мјерењем рефлексије била је 5,37 eV.

Кључне ријечи: La_2O_3 , синтеза са недостатком растварача, наночестице.

Paper received: 9 August 2021

Paper accepted: 23 February 2022
